

Control of Photoinduced Electron Transfer in Zinc Phthalocyanine–Perylenediimide Dyad and Triad by the Magnesium Ion

Shunichi Fukuzumi,^{*,†} Kei Ohkubo,[†] Javier Ortiz,[‡] Ana M. Gutiérrez,[‡]
Fernando Fernández-Lázaro,^{*,‡} and Ángela Sastre-Santos^{*,‡}

Department of Material and Life Science, Graduate School of Engineering, Osaka University, SORST, Japan Science and Technology Agency (JST), Suita, Osaka 565-0871, Japan, and División de Química Orgánica, Instituto de Bioingeniería, Universidad Miguel Hernández, Elche 03202, Spain

Received: June 20, 2008; Revised Manuscript Received: August 12, 2008

Photoexcitation of a zinc phthalocyanine–perylene diimide (ZnPc–PDI) dyad and a bis(zinc phthalocyanine)–perylene diimide [(ZnPc)₂–PDI] triad results in formation of the triplet excited state of the PDI moiety without the fluorescence emission, whereas addition of Mg²⁺ ions to the dyad and triad results in formation of long-lived charge-separated (CS) states (ZnPc^{•+}–PDI^{•−}/Mg²⁺ and (ZnPc)₂^{•+}–PDI^{•−}/Mg²⁺) in which PDI^{•−} forms a complex with Mg²⁺. Formation of the CS states in the presence of Mg²⁺ was confirmed by appearance of the absorption bands due to ZnPc^{•+} and PDI^{•−}/Mg²⁺ complex in the time-resolved transient absorption spectra of the dyad and triad. The one-electron reduction potential (*E*_{red}) of the PDI moiety in the presence of a metal ion is shifted to a positive direction due to the binding of Mg²⁺ to PDI^{•−}, whereas the one-electron oxidation potential of the ZnPc moiety remains the same. The binding of Mg²⁺ to PDI^{•−} was confirmed by the ESR spectrum, which is different from that of PDI^{•−} without Mg²⁺. The energy of the CS state (ZnPc^{•+}–PDI^{•−}/Mg²⁺) is determined to be 0.79 eV, which becomes lower than that of the triplet excited state (ZnPc–³PDI*: 1.07 eV). This is the reason why the long-lived CS states were attained in the presence of Mg²⁺ instead of the triplet excited state of the PDI moiety.

Introduction

Photoinduced electron transfer in donor–acceptor molecules has been extensively studied, in particular for covalently linked dyads in solution as model systems of natural photosynthesis to harvest efficiently solar energy.^{1–6} A number of carefully designed energy- and electron-transfer cascades that mimic the steps occurring in natural photosynthesis have also been investigated in great detail in molecular triads, tetrads, and more extended arrays containing different photoactive and redox-active chromophores, affording long-lived charge-separated states.^{6–8} Upon selective light illumination of a given chromophore, such multicomponent model systems are able to undergo directional multistep electron and/or energy-transfer processes. Among them, the diimides of the perylene tetracarboxylic acid, referred to as perylene diimides or PDIs,⁹ are of great interest in many different scientific and technological areas. These molecules are well-known red pigments with outstanding stability, high absorption in the 400–600 nm region, and fluorescence quantum yields close to 1. Moreover, they are electron acceptors widely used as electron transporting materials in technological devices.¹⁰

On the other hand, phthalocyanines (Pcs),¹¹ have also received significant attention in view of their magnificent absorption in the 600–700 nm region, leading to a blue-coloring ability, which is accompanied by a robust nature and a likely tendency as electron donors (in case appropriate substituents are present). The latter characteristic explains the extensive use of Pcs as hole transporting material in devices.¹² There have been a

number of reports on energy-transfer processes between Pcs and PDI moieties of Pcs–PDI linked molecules.^{13–16}

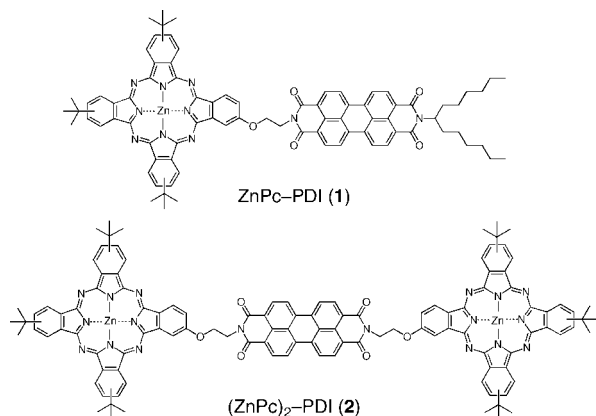
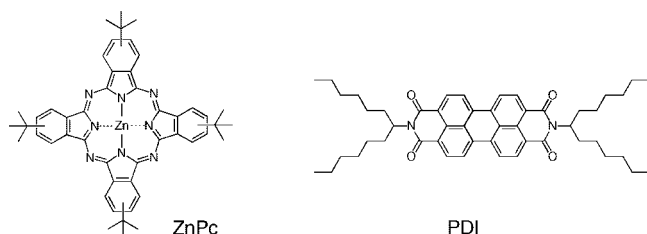
Despite the excellent light harvesting properties of both Pcs and PDIs dyes, their combination as donor–acceptor ensembles still remains challenging, because the low lying triplet excited state of PDI, which is generally lower in energy than the charge-separated (CS) state, has precluded to attain the long-lived CS state.¹⁴ A way to overcome this situation, already reported in a variety of intermolecular and intramolecular electron-transfer systems,^{17–22} is the stabilization of the CS state, thus lowering its energetic content, by complexation of radical anions, produced in the electron transfer, with metal ions which act as Lewis acids. Quantitative measurements to determine the Lewis acidity of a variety of metal ions have now been established in relation with the promoting effects of metal ions on the electron-transfer reactions.²³ Using this strategy, recently, we have reported preliminary results on the possibility to opt either for energy transfer or for electron transfer in the same perylene–phthalocyanine ensemble just by the absence or presence of magnesium ion (Mg²⁺).²⁴

We report herein the synthesis of both a perylenediimide–phthalocyanine dyad ZnPc–PDI (**1**) and its extended analogue, namely bis(zinc phthalocyanine)–perylene diimide triad (ZnPc)₂–PDI (**2**) (Chart 1) and the effects of Mg²⁺ on photoinduced electron transfer in detail. The PDI moiety containing a carbonyl oxygen plays an important role to bind with Mg²⁺ in the radical anion state (PDI^{•−}). The driving force of back electron transfer from the PDI^{•−} to the ZnPc^{•+} moiety can be controlled by addition of Mg²⁺ that can bind with PDI^{•−}. The strong binding of Mg²⁺ with PDI^{•−} results in a decrease in the CS energy and an increase in the reorganization energy of electron transfer to increase the CS lifetime. Thus, the present

* To whom correspondence should be addressed. E-mail: S.F., fukuzumi@chem.eng.osaka-u.ac.jp, F.F.-L., fdofdez@umh.es, A.S.-S., asastre@umh.es.

[†] Osaka University. Fax: +81-6-6879-7370. Tel: +81-6-6879-7368.

[‡] Universidad Miguel Hernández.

CHART 1: Drawing of ZnPc–PDI Dyad and (ZnPc)₂–PDI Triad**CHART 2: ZnPc Reference Compound and PDI Reference Compound**

study provides a new strategy to attain long-lived CS states in the Marcus normal region with a large reorganization energy.

Experimental Section

General Information. All chemicals were reagent-grade, purchased from commercial sources, and used as received, unless otherwise specified. All solvents were purified using standard procedures. Column Chromatography: SiO₂ (40–63 μm). TLC plates coated with SiO₂ 60F254 were visualized by UV light. UV–vis spectra were recorded with a Helios Gamma spectrophotometer and IR spectra with a Nicolet Impact 400D spectrophotometer. NMR spectra were measured with a Bruker AC 300 and with a Bruker AVANCE DRX-500 at room temperature. Mass spectra were obtained from a Bruker Reflex III matrix-assisted laser desorption/ionization time-of-flight (MALDI-TOF) spectrometer. Time-resolved fluorescence spectra were measured by a Photon Technology International GL-3300 with a Photon Technology International GL-302, nitrogen laser/pumped dye laser system, equipped with a four channel digital delay/pulse generator (Stanford Research System Inc. DG535) and a motor driver (Photon Technology International MD-5020). Excitation wavelength was 431 nm using 1,4-di(5-phenyl-2-oxazolyl)benzene, POPOP (Wako Pure Chemical Ind. Ltd., Japan) as a dye. Fluorescence lifetimes were determined by an exponential curve fit using a microcomputer. Elemental analyses were performed on a Thermo Finnigan Flash 1112 CHN elemental analyzer. Tetra-*tert*-butylphthalocyanine (ZnPc)²⁵ and *N,N*-bis(hexylheptyl)perylene diimide (PDI)²⁶ used as reference compounds were prepared according to previously reported procedures (Chart 2).

2-[(*tert*-Butoxycarbonyl)amino]ethanol. Di-*tert*-butyl dicarbonate (10.83 g, 48 mmol) was dissolved in tetrahydrofuran (120 mL), and 2-aminoethanol (5.89 mL, 96 mmol) was slowly added for 10 min. The mixture was stirred for 4 h at room temperature, and then the solvent was removed at reduced

pressure. The crude oil was dissolved in ethyl acetate (120 mL), washed with water (3 × 20 mL) and brine (20 mL) and dried over anhydrous MgSO₄. The solvent was removed at reduced pressure obtaining the desired compound as colorless oil (6.88 g, 89%). ¹H NMR (CDCl₃): δ = 1.45 [s, 9H, (CH₃)₃C], 2.56 (br s, 1H, OH), 3.29 (q, 2H, *J* = 5.0, CH₂N), 3.70 (t, 2H, *J* = 5.0, CH₂O), 4.99 (br s, 1H, NH).

4-{2'-[(*tert*-Butoxycarbonyl)amino]ethoxy}phthalonitrile (6).

A suspension of 4-nitrophthalonitrile (2.38 g, 13.8 mmol), [2-(*tert*-butoxycarbonyl)amino]ethanol (6.88 g, 42.8 mmol) and potassium carbonate (4.75 g, 34.4 mmol) in anhydrous dimethylformamide (26 mL), was stirred for 24 h at room temperature under argon. Then the crude mixture was poured into water and the aqueous phase was extracted with ethyl acetate (3 × 20 mL). The combined extracts were washed with water and then dried over anhydrous Na₂SO₄. The solvent was removed at reduced pressure, and the residue was dissolved in a refluxing mixture of hexane (24 mL) and ethyl acetate (12 mL). The cooled solution was introduced in an ice–water bath and stirred vigorously for 2 h. The precipitate was filtered off, washed with pentane and dried (2.49 g, 62%). Mp: 90 °C. ¹H NMR (CDCl₃): δ = 1.45 [s, 9H, (CH₃)₃C], 3.58 (q, *J* = 5.7 Hz, 2H, CH₂N), 4.14 (t, *J* = 5.2, 2H, CH₂O), 4.98 (br s, 1H, NH), 7.22 (dd, *J* = 8.8 and 2.8, 1H, ArH), 7.29 (d, *J* = 2.8, 1H, ArH), 7.73 (d, *J* = 8.8, 1H, ArH). ¹³C NMR (CDCl₃): δ = 28.25 [(CH₃)₃C], 39.5 (CH₂N), 68.2 (CH₂O), 79.8 [(CH₃)₃C], 107.4, 115.1, 115.6, 117.3, 119.2, 119.8, 135.3, 155.7 (CO₂), 161.7. IR (Ge-ATR): ν = 3355, 2232, 1668, 1257, 1166 cm⁻¹. EI-MS: *m/z* (%) = 231 (M⁺ – 56), 213 (8), 187(5), 170 (2), 157 (12), 144 (9), 127 (14), 115 (3), 100 (11), 88, (31), 70 (25), 57 (100). Anal. Calcd for C₁₅H₁₇N₃O₃: C, 62.71; H, 5.96; N, 14.63%. Found: C, 62.61; H, 6.00; N, 14.54%.

2-{2'-[(*tert*-Butoxycarbonyl)amino]ethoxy}-9,16,23-tri-*tert*-butylphthalocyaninato Zinc(II) (7). A mixture of compound **6** (200 mg, 0.696 mmol), 4-*tert*-butylphthalonitrile (385 mg, 2.09 mmol), Zn(CH₃CO₂)₂·2H₂O (306 mg, 1.39 mmol), 2 drops of 1,5-diazabicyclo[4.3.0]non-5-ene and (dimethylamino)ethanol (3.2 mL) was refluxed under argon for 5 h. The green solution obtained was cooled, and 40 mL of toluene was added. The solvent was removed and the crude product was purified by column chromatography (hexanes/AcOEt = 4/1) affording pure **7** (58 mg, 9%). ¹H NMR (DMSO-*d*₆): δ = 1.48, 1.49 [2 br s, 9H, (CH₃)₃CO], 1.76–1.79 [m, 27H, (CH₃)₃CAr], 3.63 (br q, *J* = 5.5, 2H, CH₂N), 4.60 (m, 2H, CH₂O), 7.29 (m, 1H, NH), 7.82 (m, 1H, ArH), 8.36 (m, 3H, ArH), 8.92 (m, 1H, ArH), 9.28–9.49 (m, 7H, ArH); IR (KBr): ν = 2957, 2903, 2867, 1697, 1644, 1489, 1392, 1332, 1090, 747 cm⁻¹. UV–vis (DMF): λ_{max} (log ε) = 677 (5.35), 610 (4.59), 350 nm (4.90). MALDI-TOF-MS (dithranol): *m/z* = 903 (M⁺). Anal. Calcd for C₅₁H₅₃N₉O₃Zn·H₂O: C, 66.33; H, 6.00; N, 13.65%. Found: C, 66.09; H, 5.91; N, 13.61%.

2-(2'-Aminoethoxy)-9,16,23-tri-*tert*-butylphthalocyaninato Zinc(II) (3). Phthalocyanine **7** (30 mg, 0.033 mmol) was dissolved in a mixture of dichloromethane (0.3 mL) and trifluoroacetic acid (0.3 mL) at 0 °C for 2 h. The solvent was removed, the residue was treated with 2 M sodium hydroxide solution, extracted with ethyl acetate (3 × 5 mL) and washed with water (2 × 3 mL) affording **3** (22 mg, 83%). ¹H NMR (TFA-*d*₁): δ = 1.80 [s, 27H, (CH₃)₃C], 4.04 (m, 2H, CH₂N), 4.96 (m, 2H, CH₂O), 8.00 (m, 1H, ArH), 8.59–8.64 (m, 3H, ArH), 9.15–9.18 (m, 1H, ArH), 9.42–9.50 (m, 4H, ArH), 9.58–9.67 (m, 3H, ArH); IR (KBr): ν = 2957, 2904, 2866, 1611, 1489, 1393, 1331, 1090, 748 cm⁻¹. UV–vis (DMF): λ_{max}

(log ϵ) = 677 (5.33), 610 (4.59), 350 nm (4.89). MALDI-TOF-MS (dithranol): m/z = 803 (M^+).

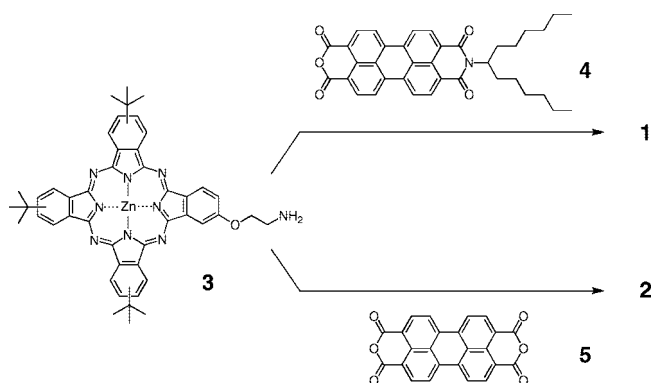
***N*-{2'-[9'',16'',23''-tri-*tert*-butylphthalocyaninato zinc(II)-2''-yl]oxyethyl}-*N'*-(2''-hexylheptyl)perylene-3,4:9,10-bis(dicarboximide) (1).** *N*-(1'-Hexylheptyl)perylene-3,4-dicarboxyanhydride-9,10-dicarboximide (50 mg, 0.087 mmol) and phthalocyanine **3** (70 mg, 0.087 mmol) were heated 7 h at 170 °C in imidazole (320 mg). After cooling, the solid was washed by centrifugation with methanol (2 × 10 mL), until the supernatant was pale pink. The solid was chromatographed (SiO₂, CH₂Cl₂/AcOEt = 9/1) yielding **1** (57 mg, 48%). ¹H-RMN (TFA-*d*₁): δ = 0.90 (br s, 6H), 1.25–1.55 (m, 14H), 1.75–1.95 (m, 27H), 2.05–2.45 (2m, 6H), 5.10–5.50 (m, 5H), 7.90–9.70 (m, 20H, ArH); IR (KBr): ν = 2955, 2925, 2859, 1696, 1658, 1594, 1340, 1090, 747 cm⁻¹. UV-vis (DMF): λ_{\max} (log ϵ) = 679 (5.17), 614 (4.41), 533 (4.72), 494 (4.46), 464 (4.10), 353 nm (4.82). MALDI-TOF-MS (dithranol): m/z = 1358 (M^+). Anal. Calcd for C₈₃H₇₈N₁₀O₅Zn·2H₂O: C, 71.36; H, 5.92; N, 10.03%. Found: C, 71.15; H, 5.73; N, 10.13%.

***N,N'*-Bis{2'-[9'',16'',23''-tri-*tert*-butylphthalocyaninato zinc(II)-2''-yl]oxyethyl}perylene-3,4:9,10-bis(dicarboximide) (2).** Perylene-3,4,9,10-tetracarboxylic acid bisanhydride (4.9 mg, 0.0124 mmol) and phthalocyanine **3** (20 mg, 0.025 mmol) were heated 7.5 h at 155 °C in imidazole (174 mg). After cooling, the solid was washed by sonication with methanol (2 × 6 mL), until the supernatant was pale pink. After drying under vacuum, the solid was chromatographed (SiO₂, CH₂Cl₂/MeOH = 98/2) to yield **2** (12 mg, 49%). ¹H-RMN (TFA-*d*₁): δ = 1.82, 1.90 [2 br s, 54H, 6x(CH₃)₃C], 4.82–4.98, 5.00–5.14 (2m, 8H, 4×CH₂), 7.60–9.70 (3m, 32H, ArH). IR (KBr): ν = 2955, 1697, 1660, 1594, 1489, 1362, 1332, 1283, 1256, 1090, 1047, 747 cm⁻¹. UV-vis (DMF): λ_{\max} (log ϵ) = 677 (5.28), 617 (4.59), 543 (4.70), 501 (4.27), 350 nm (5.03). MALDI-TOF-MS (dithranol): m/z = 1967 ([M + H]⁺).

Cyclic Voltammetry. Electrochemical measurements were performed on an ALS630B electrochemical analyzer in deaerated MeCN containing 0.1 M Bu₄NPF₆ (TBAPF₆) as supporting electrolyte at 298 K. A conventional three-electrode cell was used with a platinum working electrode (surface area of 0.3 mm²) and a platinum wire as the counter electrode. The Pt working electrode (BAS) was routinely polished with BAS polishing alumina suspension and rinsed with acetone before use. The measured potentials were recorded with respect to the Ag/AgNO₃ (0.01 M) reference electrode. All potentials (vs Ag/Ag⁺) were converted to values vs SCE by adding 0.29 V.²⁷ All electrochemical measurements were carried out under an atmospheric pressure of Ar.

Laser Flash Photolysis. An MeCN solution containing ZnPc-PDI was excited by a Panther OPO pumped by Nd:YAG laser (Continuum, SLII-10, 4–6 ns fwhm) with the powers of 1.5 and 3.0 mJ per pulse. The transient absorption measurements were performed using a continuous xenon lamp (150 W) and an InGaAs-PIN photodiode (Hamamatsu 2949) as a probe light and a detector, respectively. The output from the photodiodes and a photomultiplier tube was recorded with a digitizing oscilloscope (Tektronix, TDS3032, 300 MHz). Femtosecond transient absorption spectroscopy experiments were conducted using an ultrafast source: Integra-C (Quantronix Corp.), an optical parametric amplifier: TOPAS (Light Conversion Ltd.) and a commercially available optical detection system: Helios provided by Ultrafast Systems LLC. The source for the pump and probe pulses were derived from the fundamental output of Integra-C (780 nm, 2 mJ/pulse and fwhm = 130 fs) at a repetition rate of 1 kHz. A total of 75% of the fundamental

SCHEME 1



output of the laser was introduced into TOPAS, which has optical frequency mixers resulting in tunable range from 285 to 1660 nm, whereas the rest of the output was used for white light generation. Typically, 2500 excitation pulses were averaged for 5 s to obtain the transient spectrum at a set delay time. Kinetic traces at appropriate wavelengths were assembled from the time-resolved spectral data. All measurements were conducted at 298 K. The transient spectra were recorded using fresh solutions in each laser excitation.

ESR Measurements. The ESR spectra were recorded at low temperature on a JEOL X-band ESR spectrometer (JES-ME-LX). A quartz ESR tube (internal diameter: 5.5 mm) containing an oxygen-saturated solution of (BNA)₂ containing NH₄PF₆ or Bu₄NPF₆ at 143 K was irradiated in the cavity of the ESR spectrometer with the focused light of a 1000 W high-pressure Hg lamp (Ushio-US1005D) through an aqueous filter. The ESR spectra were measured under nonsaturating microwave power conditions. The amplitude of modulation was chosen to optimize the resolution and the signal-to-noise (*S/N*) ratio of the observed spectra. The *g* values were calibrated with a Mn²⁺ marker.

Theoretical Calculations. Density-functional theory (DFT) calculations were performed on a COMPAQ DS20E computer. Geometry optimizations were carried out using the Becke3LYP functional and 6-31G(d) basis set,^{28–30} with the unrestricted Hartree-Fock (UHF) formalism and as implemented in the Gaussian 03 program Revision C.02. Graphical outputs of the computational results were generated with the Gauss View software program (ver. 3.09) developed by Semichem, Inc.

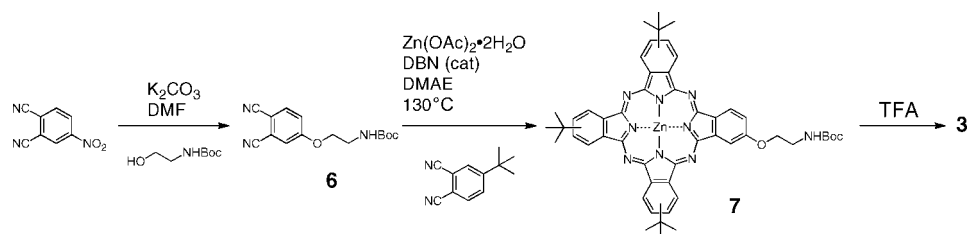
Results and Discussion

Synthesis. Perylenediimide-phthalocyanine arrays **1–2** were synthesized as indicated in Scheme 1 by condensation of the corresponding aminotri-*tert*-butyl phthalocyanine **3** with either the monoanhydride **4** or the bisanhydride **5** at high temperature using melted imidazole as solvent.

The synthesis of the phthalocyanine **3** was accomplished by the first time as depicted in Scheme 2. Ipso substitution in 4-nitrophthalonitrile with 2-[(*tert*-butoxycarbonyl)amino]ethanol gives rise to 4-{2'-[(*tert*-butoxycarbonyl)amino]ethoxy}phthalonitrile (**6**) in a good yield. Statistical condensation of phthalonitrile **6** with 4-*tert*-butylphthalonitrile in the presence of zinc as template, under the usual conditions to obtain unsymmetrically substituted phthalocyanines, yields the new amino Boc-protected phthalocyanines, yields the new amino Boc-protected phthalocyanine **7**. Treatment with trifluoroacetic acid afforded the (2-aminoethoxy)tri-*tert*-butylphthalocyanine **3** with 83% yield.

Spectroscopic and Redox Properties. ZnPc has absorption maxima at 613 and 680 nm, whereas PDI has absorption maxima at 462, 493 and 529 nm as shown in Figure 1a,b,

SCHEME 2



respectively. The absorption spectra of ZnPc–PDI (**1**) and (ZnPc)₂–PDI (**2**) are virtually the superposition of the spectrum of each component (ZnPc and PDI) as shown in Figure 1c, where the absorption maxima (462, 494, 531, 616 and 682 nm for ZnPc–PDI and 476, 497, 542, 481 for (ZnPc)₂–PDI) are slightly red-shifted. Thus, there is little interaction between the ZnPc and PDI moieties in the ground states.

Cyclic voltammograms of ZnPc–PDI, ZnPc, and PDI are shown in Figure 2a–c, respectively. The one-electron redox waves of ZnPc–PDI are virtually the superposition of those of ZnPc and PDI, although the redox potentials are slightly shifted to positive direction in the dyad as compared to those of each component. The cyclic voltammogram and differential pulse voltammogram of (ZnPc)₂–PDI are shown in Figure 3a,b, respectively. On the basis of the oxidation potential of the ZnPc moiety and the reduction potential of the PDI moiety, the energies of the CS states, ZnPc^{•+}–PDI^{•-} and (ZnPc)₂^{•+}–PDI^{•-}, are estimated as 1.21 and 1.25 eV, respectively.

Photodynamics of ZnPc–PDI Dyad. The photoexcitation of ZnPc and PDI affords the fluorescence emission of ¹ZnPc* at 694 nm,³¹ and that of ¹PDI* at 544 nm, as shown in Figure 4. The fluorescence lifetimes of ZnPc and PDI were determined as 3.2 and 4.2 ns in deaerated PhCN, respectively. In the case of ZnPc–PDI, however, the photoexcitation of the absorption band of the ZnPc and PDI moieties results in no fluorescence emission.

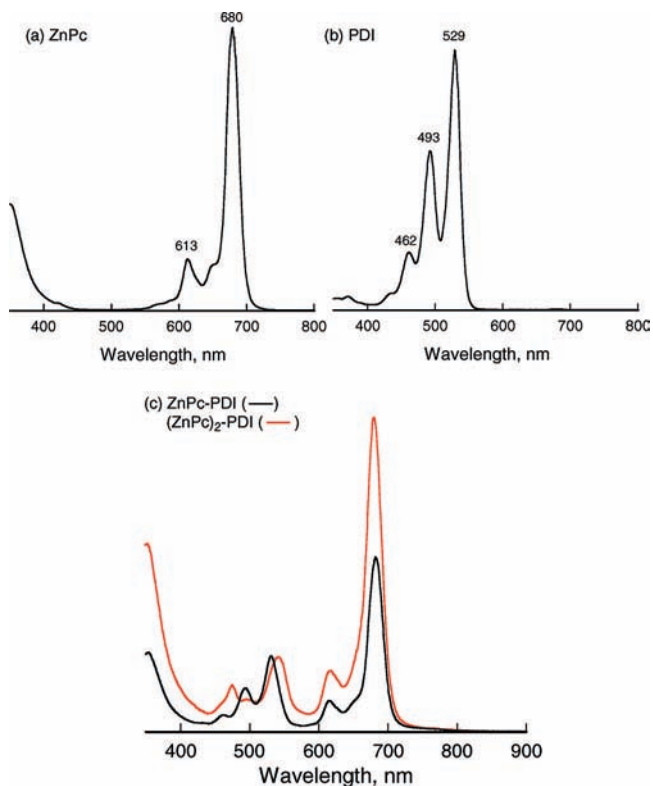


Figure 1. UV–vis absorption spectra of (a) ZnPc, (b) PDI and (c) ZnPc–PDI (black) and (ZnPc)₂–PDI (red) in PhCN at 298 K.

The triplet energies of ZnPc and PDI were determined from emission maxima of phosphorescence spectra in butyronitrile containing 10 mM methyl iodide (1050 nm for ZnPc and 1160 nm for PDI in Figure 5).^{32,33}

Laser excitation of the absorption band at 530 nm due to the PDI moiety of ZnPc–PDI at 530 nm results in formation of the triplet excited state of state of ZnPc (³ZnPc*–PDI) in deaerated benzonitrile (PhCN) via energy transfer from ¹PDI* to ZnPc, followed by intersystem crossing as reported previously.²⁴ The triplet–triplet (T–T) absorption at 510 nm due to ³ZnPc*–PDI is changed to the T–T absorption at 700 nm due to the triplet excited state of PDI (ZnPc–³PDI*).²⁴ The decay of the T–T absorption at 510 nm due to ³ZnPc*–PDI coincides with the rise in the T–T absorption at 710 nm due to ZnPc–³PDI* (Figure 6a). The rate constant of energy transfer from ³ZnPc* to the PDI moiety in ZnPc–PDI is determined at

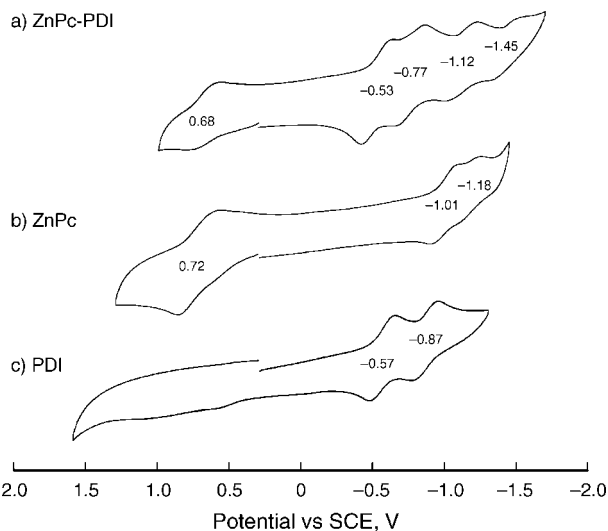


Figure 2. Cyclic voltammograms of (a) ZnPc–PDI (1.0×10^{-3} M), (b) ZnPc (1.0×10^{-3} M), and (c) PDI (1.0×10^{-3} M) in deaerated PhCN containing TBAPF₆ (0.1 M) at 298 K. Sweep rate: 50 mV s⁻¹.

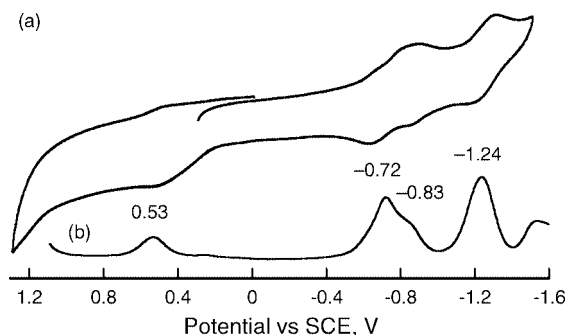


Figure 3. (a) Cyclic voltammogram and (b) differential pulse voltammogram of (ZnPc)₂–PDI (2.0×10^{-4} M) in deaerated PhCN containing TBAPF₆ (0.1 M) at 298 K. Sweep rate: 50 mV s⁻¹ for CV and 4 mV s⁻¹ for DPV.

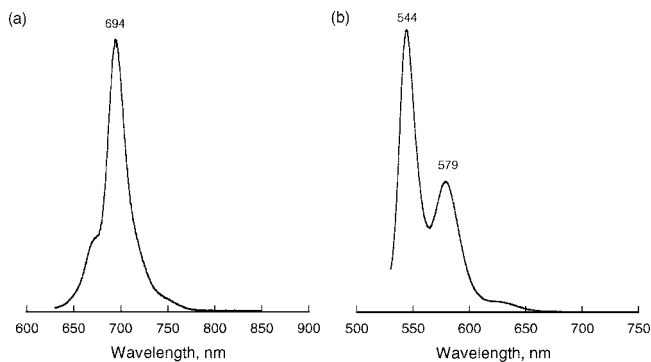


Figure 4. Fluorescence spectra of (a) ZnPc ($\lambda_{\text{ex}} = 610$ nm) and (b) PDI ($\lambda_{\text{ex}} = 530$ nm) in deaerated PhCN at 298 K.

298 K as $2.0 \times 10^4 \text{ s}^{-1}$. The T-T absorption due to $\text{ZnPc}-{}^3\text{PDI}^*$ decays at a longer time scale (Figure 6b) and the decay rate constant ($6.4 \times 10^2 \text{ s}^{-1}$) agrees with that of the T-T absorbance of the reference compound (PDI).

Photodynamics of $(\text{ZnPc})_2$ -PDI Triad. Time-resolved transient absorption spectra of $(\text{ZnPc})_2$ -PDI were measured by femtosecond laser photolysis in deaerated PhCN. A transient absorption spectrum observed after the femtosecond laser pulse excitation of a PhCN solution of $(\text{ZnPc})_2$ -PDI is shown in Figure 7a. The transient absorption bands at 720, 766, 795 and 955 nm are those of characteristic $\text{PDI}^{\bullet-}$ bands.³⁴ The absorption bands at 520 and 850 nm are assigned to those due to $\text{ZnPc}^{\bullet+}$, accordingly to data shown in Figure 8, where $\text{ZnPc}^{\bullet+}$ was produced by the electrochemical oxidation of ZnPc at the applied potential of 0.80 V vs SCE. The bleaching observed at 494 and

531 nm are due to ${}^1\text{PDI}^*$ and that at 613 and 682 nm are due to ${}^1\text{ZnPc}^*$. Thus, the photoexcitation of the PDI moiety of $(\text{ZnPc})_2$ -PDI at $\lambda = 450$ nm results in electron transfer from ZnPc to ${}^1\text{PDI}^*$ together with electron transfer from ${}^1\text{ZnPc}^*$, which is produced by energy transfer from ${}^1\text{PDI}^*$ to ZnPc, to PDI to produce the CS state, $(\text{ZnPc})_2^{\bullet+}-\text{PDI}^{\bullet-}$. The decay of the CS state is monitored at 740 nm (Figure 7b). The lifetime of the CS state is determined to be 14 ps, which is much shorter than the time scale of the intersystem crossing to afford the triplet excited state of ZnPc (${}^3\text{ZnPc}^*$). Thus, the decay of the CS state affords ${}^3\text{ZnPc}^*$ prior to the intersystem crossing from ${}^1\text{ZnPc}^*$ (vide infra).

The formation of ${}^3\text{ZnPc}^*$ is confirmed by nanosecond laser excitation of $(\text{ZnPc})_2$ -PDI at 545 nm in which only the PDI moiety absorbs the light (see Figure 1). The resulting transient absorption spectra are shown in Figure 9, where the triplet-triplet (T-T) absorption band due to ${}^3\text{ZnPc}^*$ is observed at 470 nm together with the bleaching that corresponds to the absorption bands of ZnPc. The T-T absorption band due to ${}^3\text{ZnPc}^*$ decays accompanied by a rise in the T-T absorption band at 710 nm due to ${}^3\text{PDI}^*$ in the triad, which agrees with the T-T absorption of the reference compound (${}^3\text{PDI}^*$).

The energy diagram of photodynamics of $(\text{ZnPc})_2$ -PDI is summarized in Scheme 3. The photoexcitation of the PDI moiety of $(\text{ZnPc})_2$ -PDI results in energy transfer from ${}^1\text{PDI}^*$ to ZnPc and electron transfer from ZnPc to ${}^1\text{PDI}^*$ to produce the CS state, $(\text{ZnPc})_2^{\bullet+}-\text{PDI}^{\bullet-}$. The CS state is the singlet state and decays via back electron transfer to the ground state and ${}^3(\text{ZnPc})_2^*-\text{PDI}$. Because the CS state initially formed is the singlet state, the back electron transfer to ${}^3(\text{ZnPc})_2^*-\text{PDI}$

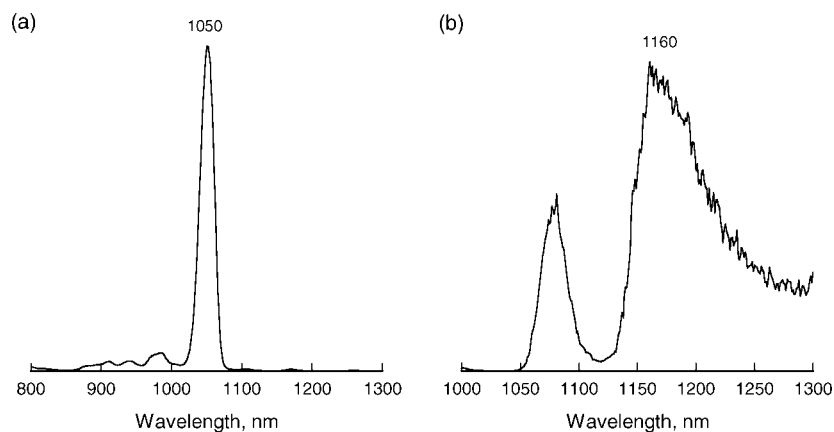


Figure 5. Phosphorescence spectra of (a) ZnPc ($\lambda_{\text{ex}} = 610$ nm) and (b) PDI ($\lambda_{\text{ex}} = 530$ nm) in argon-saturated glassy butyronitrile containing MeI (10 mM) at 77 K.

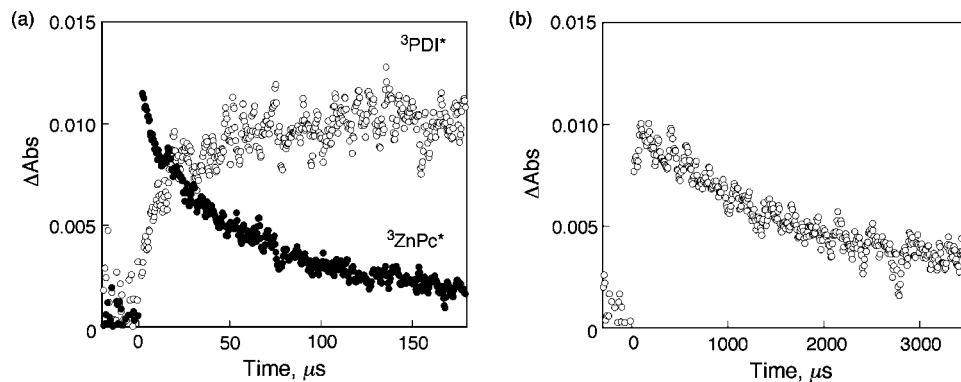


Figure 6. (a) Decay and risetime profiles of transient absorption of ZnPc-PDI at 510 (●) and 710 nm (○) (short time scale). (b) Decay time profile at 710 nm (long time scale).

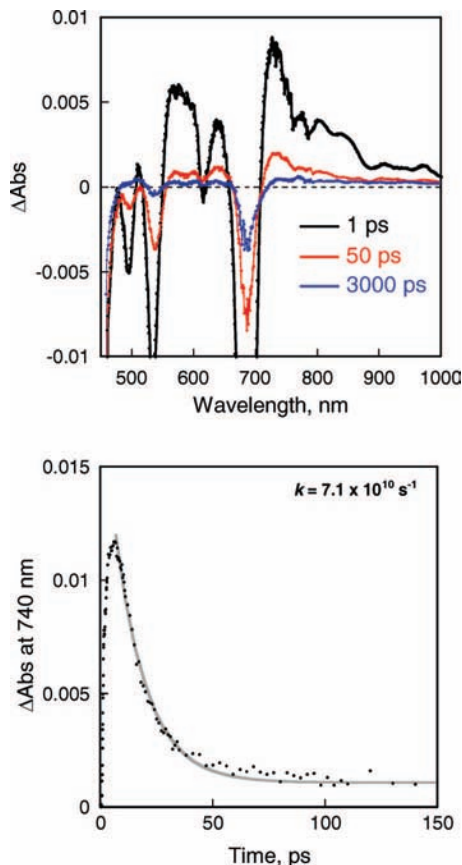


Figure 7. (a) Transient absorption spectra of $(\text{ZnPc})_2\text{-PDI}$ in deaerated PhCN taken by femtosecond laser excitation at 450 nm. (b) Time profile of the absorbance at 740 nm.

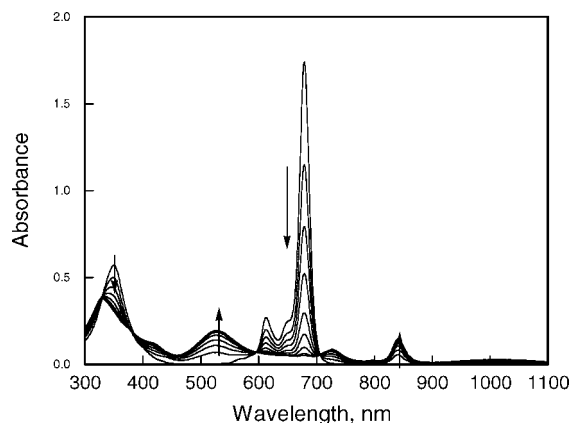


Figure 8. Spectral change in the electrochemical oxidation of ZnPc in deaerated PhCN containing TBAPF₆ (0.1 M) at the applied potential of 0.80 V vs SCE at 298 K.

requires a spin-orbit-intersystem crossing.³⁵ The spin-orbit interaction may be much stronger with $^3(\text{ZnPc})_2^*\text{-PDI}$ as compared with $(\text{ZnPc})_2\text{-}^3\text{PDI}^*$, because the smaller energy difference between $(\text{ZnPc})_2^{*+}\text{-PDI}^{*-}$ and $^3(\text{ZnPc})_2^*\text{-PDI}$ (0.07 eV) as compared with the energy difference between $(\text{ZnPc})_2^{*+}\text{-PDI}^{*-}$ and $(\text{ZnPc})_2\text{-}^3\text{PDI}^*$ (0.18 eV). This may be the reason why the decay of the CS state affords $^3(\text{ZnPc})_2^*\text{-PDI}$ rather than $(\text{ZnPc})_2\text{-}^3\text{PDI}^*$. Then energy transfer occurs from $^3\text{ZnPc}^*$ to PDI to produce $(\text{ZnPc})_2\text{-}^3\text{PDI}^*$. Because the CS state (1.25 eV) is higher in energy than the triplet excited state ($^3\text{ZnPc}^*\text{-PDI}$), no long-lived CS state was observed in the transient absorption spectrum. This demonstrates sharp contrast

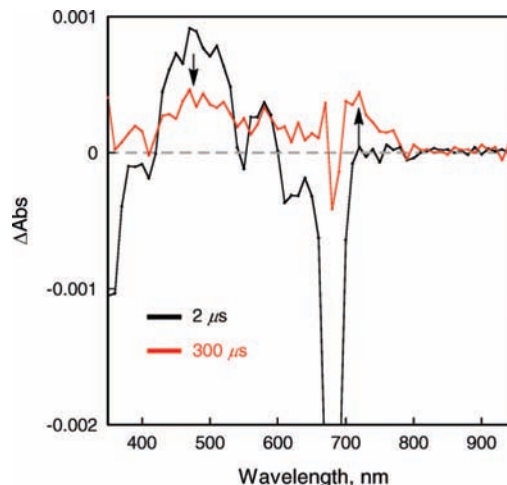
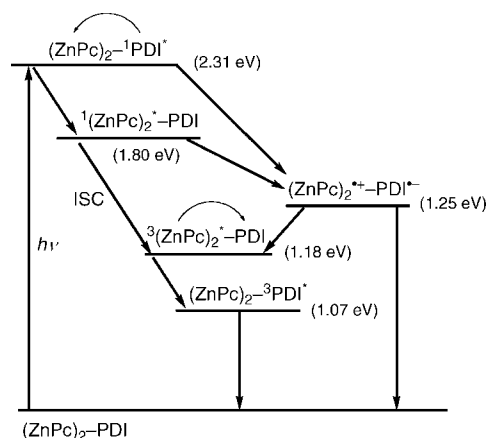


Figure 9. Transient absorption spectra of $(\text{ZnPc})_2\text{-PDI}$ (2.0×10^{-5} M) obtained by nanosecond laser flash photolysis in deaerated PhCN at 298 K at 2 and 300 μs after laser excitation ($\lambda = 545$ nm).

SCHEME 3



with the case of zinc porphyrin–PDI dyad which affords the CS state upon the photoexcitation.^{36,37}

Effects of Mg^{2+} on Photodynamics of $(\text{ZnPc})_2\text{-PDI}$. In contrast to the above case, the addition of magnesium perchlorate [$\text{Mg}(\text{ClO}_4)_2$] (0.10 M) to a PhCN solution of $(\text{ZnPc})_2\text{-PDI}$ and the photoexcitation at 545 nm results in formation of the

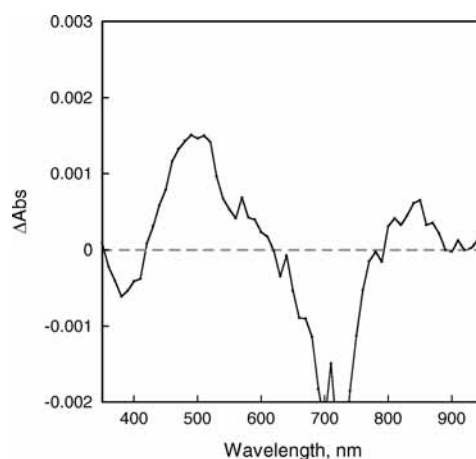


Figure 10. Transient absorption spectra of $(\text{ZnPc})_2\text{-PDI}$ (2.0×10^{-5} M) with $\text{Mg}(\text{ClO}_4)_2$ (0.10 M) obtained by nanosecond laser flash photolysis in deaerated PhCN at 298 K at 4 μs after laser excitation ($\lambda = 545$ nm).

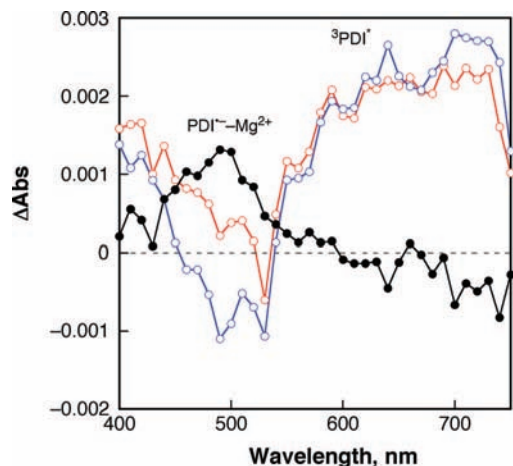


Figure 11. Transient absorption spectra observed in deaerated PhCN solution containing PDI and (BNA)₂ in the presence of Mg(ClO₄)₂ (0.1 M) at 3 μs (blue) and 300 μs (red) after laser excitation (λ = 530 nm) and the difference spectrum (black).

long-lived CS state as indicated by the appearance of the transient absorption band due to ZnPc^{•+} at 850 nm together with PDI^{•-}/Mg²⁺ complex at 500 nm (Figure 10). The formation of the CS state was confirmed by comparing the transient spectra in Figure 10 with the spectrum of ZnPc^{•+} obtained by the electrochemical oxidation of ZnPc (Figure 8) and that of the PDI^{•-}/Mg²⁺ complex produced by photoinduced electron-transfer reduction of PDI with dimeric 1,4-dihydronicotinamide [(BNA)₂]³⁸ in the presence of Mg²⁺ in deaerated PhCN (Figure 11). The absorption maximum at 500 nm in Figure 10 agrees

with the absorption maximum of the PDI^{•-}/Mg²⁺ complex (Figure 11). The absorption band due to the PDI^{•-}/Mg²⁺ complex (λ_{max} = 500 nm) is significantly shifted from that of PDI^{•-} (λ_{max} = 720 nm)³⁴ due to the complex formation with Mg²⁺, whereas no change in the absorption spectrum of PDI is observed in the presence of Mg²⁺ (0.10 M) in PhCN.³⁹

The ESR spectrum of PDI^{•-} in the presence of Mg²⁺ (0.10 M) was also changed due to the complex formation with Mg²⁺ as compared with that of PDI^{•-} in the absence of Mg²⁺ as shown in Figure 12. The hyperfine coupling (*hfc*) constants of PDI^{•-} consist of those of two equivalent nitrogens (*a*(2N) = 0.57 G) and two sets of four equivalents protons (*a*(4H) = 1.79 and 0.59 G). The *hfc* values were estimated by DFT method (B3LYP/6-31G(d) basis set) as shown in red numbers of Figure 12. The *hfc* values are significantly changed in the case of PDI^{•-}-Mg²⁺ complex: two nitrogens are inequivalent (*a*(N) = 0.31 and 0 G) and there are eight inequivalent protons as shown in the bottom at right column in Figure 12. Such inequivalent nitrogens and eight inequivalent protons can only be rationalized by 1:1 stoichiometry of Mg²⁺ binding to PDI^{•-}.⁴⁰

The one-electron reduction potential of (ZnPc)₂-PDI **2** (-0.72 V vs SCE) was shifted to -0.22 V vs SCE in the presence of Mg(ClO₄)₂ (0.10 M) due to the complex formation with Mg²⁺ in PhCN (see Supporting Information S2). The energy of the CS state ((ZnPc)₂^{•+}-PDI^{•-}/Mg²⁺) is then determined to be 0.79 eV, which is now lower than the triplet excited state energy ((ZnPc)₂-³PDI*: 1.07 eV). The quantum yield of the CS state was determined as 72% using the comparative method.⁴¹

The decay of the CS state of (ZnPc)₂-PDI **2** in the presence of Mg(ClO₄)₂ (0.1 M) obeys first-order kinetics as shown in

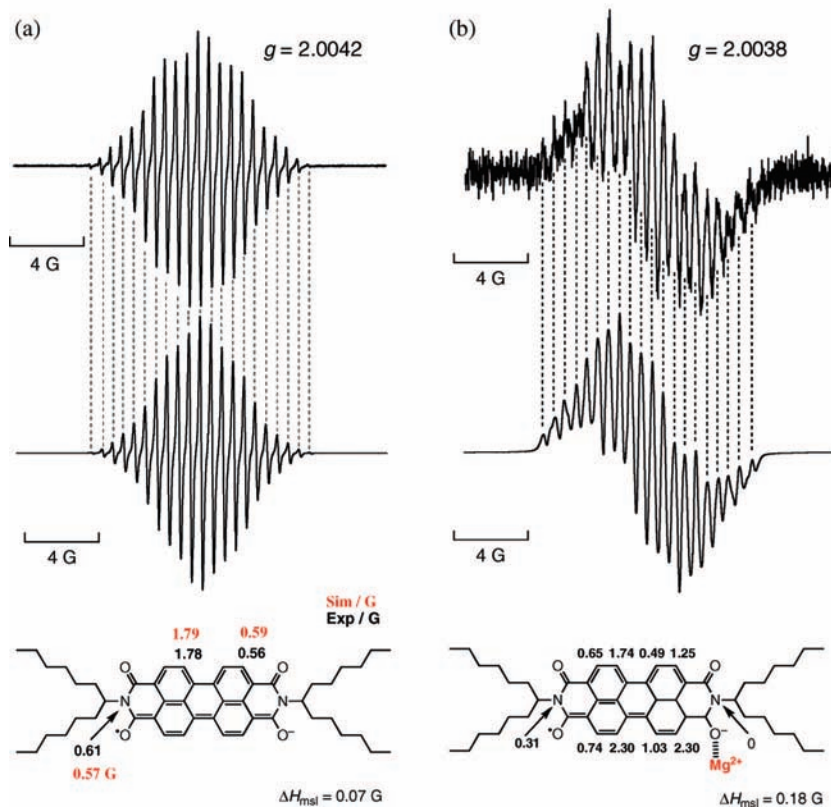


Figure 12. ESR spectra of PDI^{•-} formed in the photoinduced electron-transfer reduction of PDI (1.0 × 10⁻⁴ M) by (BNA)₂ (5.0 × 10⁻⁴ M) in the (a) absence and (b) presence of Mg(ClO₄)₂ (0.1 M) in deaerated PhCN at 298 K (top column) with the computer simulation spectra (middle column) and the hyperfine coupling constants (in G) and maximum slope line width (Δ*H*_{msl}) (bottom column). The agreement between the observed and simulated spectra is shown by the broken lines.

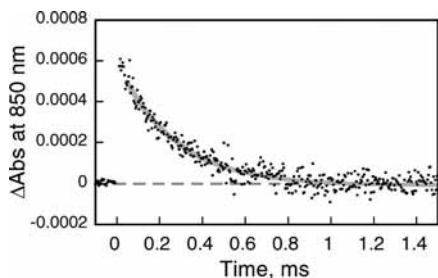


Figure 13. Decay time profile of transient absorption of $(\text{ZnPc})_2\text{-PDI}$ (2.0×10^{-5} M) with $\text{Mg}(\text{ClO}_4)_2$ (0.10 M) at 850 nm. $k_d = 3.7 \times 10^3$ s^{-1} , $\tau = 270$ μs at 298 K.

SCHEME 4

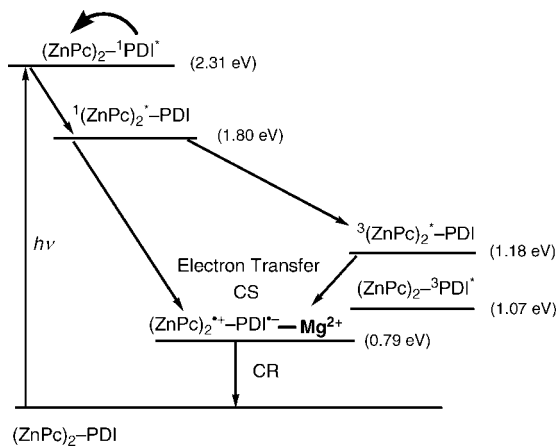


Figure 13. The first-order decay indicates that no intermolecular reaction is involved in the charge-recombination (CR) process. The lifetime of the CS state of $(\text{ZnPc})_2\text{-PDI}$ **2** was determined as 270 μs in PhCN at 298 K. Similarly the lifetime of the CS state of ZnPc-PDI **1** was determined as 240 μs in PhCN.

In conclusion, the addition of Mg^{2+} to PhCN solutions of ZnPc-PDI and $(\text{ZnPc})_2\text{-PDI}$ results in drastic change in the photodynamics from the formation of $^3\text{PDI}^*$ (Scheme 3) to electron transfer to produce the corresponding long-lived charge-separated states [$\text{ZnPc}^{+\bullet}\text{-PDI}^-/\text{Mg}^{2+}$ and $(\text{ZnPc})_2^{+\bullet}\text{-PDI}^-/\text{Mg}^{2+}$, respectively] in which PDI^- forms a complex with Mg^{2+} (Scheme 4).

Acknowledgment. We thank support from the Spanish Government CICYT and FEDER (grants MAT2005-07369-C03-02, CTQ2007-67888/BQU and Consolider Ingenio 2010 project HOPE CSD2007-00007) and a Grant-in-Aid (Nos. 19205019 and 19750034) and a Global COE program, “the Global Education and Research Center for Bio-Environmental Chemistry” from the Ministry of Education, Culture, Sports, Science and Technology, Japan.

Supporting Information Available: Calculated *hfc* values of protonated $\text{PDI}^{\bullet-}$ [$(\text{PDI-H})^{\bullet-}$] obtained by DFT at the B3LYP/6-31G(d) basis set (S1) and a differential pulse voltammogram of **2** in the presence of Mg^{2+} (S2). This material is available free of charge via the Internet at <http://pubs.acs.org>.

References and Notes

(1) (a) Gust, D.; Moore, T. A. In *The Porphyrin Handbook*; Kadish, K. M., Smith, K. M., Guillard, R., Eds.; Academic Press: San Diego, CA, 2000; Vol. 8, pp 153–190. (b) Gust, D.; Moore, T. A.; Moore, A. L. In *Electron Transfer in Chemistry*; Balzani, V., Ed.; Wiley-VCH: Weinheim, 2001; Vol. 3, pp 272–336. (c) Gust, D.; Moore, T. A.; Moore, A. L. *Acc. Chem. Res.* **2001**, *34*, 40.

(2) (a) Wasielewski, M. R. In *Photoinduced Electron Transfer*; Fox, M. A., Chanon, M., Eds.; Elsevier: Amsterdam, 1988; Part A, pp161–206. (b) Wasielewski, M. R. *Chem. Rev.* **1992**, *92*, 435.
 (3) (a) Guldi, D. M. *Chem. Soc. Rev.* **2002**, *31*, 22–36. (b) Guldi, D. M. *Chem. Commun.* **2000**, 321.
 (4) (a) Paddon-Row, M. N. *Acc. Chem. Res.* **1994**, *27*, 18. (b) Jordan, K. D.; Paddon-Row, M. N. *Chem. Rev.* **1992**, *92*, 395.
 (5) Blanco, M.-J.; Consuelo Jiménez, M.; Chambron, J.-C.; Heitz, V.; Linke, M.; Sauvage, J.-P. *Chem. Soc. Rev.* **1999**, *28*, 293.
 (6) (a) Fukuzumi, S.; Guldi, D. M. In *Electron Transfer in Chemistry*; Balzani, V., Ed.; Wiley-VCH: Weinheim, 2001; Vol. 2, pp 270–337. (b) Fukuzumi, S. *Org. Biomol. Chem.* **2003**, *1*, 609.
 (7) (a) Imahori, H.; Tamaki, K.; Guldi, D. M.; Luo, C.; Fujitsuka, M.; Ito, O.; Sakata, Y.; Fukuzumi, S. *J. Am. Chem. Soc.* **2001**, *123*, 2607. (b) Imahori, H.; Guldi, D. M.; Tamaki, K.; Yoshida, Y.; Luo, C.; Sakata, Y.; Fukuzumi, S. *J. Am. Chem. Soc.* **2001**, *123*, 6617. (c) Imahori, H.; Sekiguchi, Y.; Kashiwagi, Y.; Sato, T.; Araki, Y.; Ito, O.; Yamada, H.; Fukuzumi, S. *Chem.-Eur. J.* **2004**, *10*, 3184.
 (8) (a) Imahori, H.; Tamaki, K.; Araki, Y.; Sekiguchi, Y.; Ito, O.; Sakata, Y.; Fukuzumi, S. *J. Am. Chem. Soc.* **2002**, *124*, 5165. (b) Guldi, D. M.; Imahori, H.; Tamaki, K.; Kashiwagi, Y.; Yamada, H.; Sakata, Y.; Fukuzumi, S. *J. Phys. Chem. A* **2004**, *108*, 541.
 (9) (a) Würthner, F. *Chem. Commun.* **2004**, 1564. (b) Langhals, H. *Helv. Chim. Acta* **2005**, *88*, 1309. (c) Wasielewski, M. R. *J. Org. Chem.* **2006**, *71*, 5051.
 (10) (a) Würthner, F. *Angew. Chem.* **2001**, *113*, 1069; *Angew. Chem. Int. Ed.* **2001**, *40*, 1037. (b) Tan, L.; Curtis, M. D.; Francis, A. H. *Chem. Mater.* **2004**, *16*, 2134. (c) Tatemichi, S.; Ichikawa, M.; Koyama, T.; Taniguchi, Y. *Appl. Phys. Lett.* **2006**, *89*, 112108.
 (11) (a) *Phthalocyanines: Properties and Applications*; Leznoff, C. C., Lever, A. B. P., Eds.; VCH: Weinheim, 1989, 1993, 1996; Vols. 1–4. (b) Hanack, M.; Heckmann, H.; Polley, R. In *Methods in Organic Chemistry (Houben-Weyl)*; Schumann, E., Ed.; Thieme: Stuttgart, 1998; Vol. E 9d, p 717. (c) Rodríguez-Morgade, M. S.; de la Torre, G.; Torres, T. In *The Porphyrin Handbook*; Kadish, K. M., Smith, K. M., Guillard, R., Eds.; Academic Press: San Diego, 2003.
 (12) de la Torre, G.; Claessens, C. G.; Torres, T. *Chem. Commun.* **2007**, 2000.
 (13) (a) Miller, M. A.; Lammi, R. K.; Prathapan, S.; Holten, D.; Lindsey, J. S. *J. Org. Chem.* **2000**, *65*, 6634. (b) Li, X.; Sinks, L. E.; Rybtchinski, B.; Wasielewski, M. R. *J. Am. Chem. Soc.* **2004**, *126*, 10810.
 (14) (a) Rodríguez-Morgade, M. S.; Torres, T.; Atienza-Castellanos, C.; Guldi, D. *J. Am. Chem. Soc.* **2006**, *128*, 15145. (b) Jiménez, A. J.; Späning, F.; Rodríguez-Morgade, M. S.; Ohkubo, K.; Fukuzumi, S.; Guldi, D. M.; Torres, T. *Org. Lett.* **2007**, *9*, 2481.
 (15) (a) Liu, M. O.; Tai, C.-H.; Hu, A. T. *J. Photochem. Photobiol. A: Chem.* **2004**, *165*, 193. (b) Gao, B.; Li, Y.; Tian, H. *Supramol. Chem.* **2007**, *19*, 207. (c) Chen, Y.; Lin, Y.; El-Khouly, M. E.; Zhuang, X.; Araki, Y.; Ito, O.; Zhang, W. *J. Phys. Chem. C* **2007**, *111*, 16096.
 (16) (a) You, C.-C.; Würthner, F. *Org. Lett.* **2004**, *6*, 2401. (b) Kirmaier, C.; Yang, S. I.; Prathapan, S.; Miller, M. A.; Diers, J. R.; Bacian, D. F.; Lindsey, J. S.; Holten, D. *Res. Chem. Intermed.* **2002**, *28*, 719. (c) Yang, S. I.; Lammi, R. K.; Prathapan, S.; Miller, M. A.; Seth, J.; Diers, J. R.; Bacian, D. F.; Lindsey, J. S.; Holten, D. *J. Mater. Chem.* **2001**, *11*, 2420. (d) Gosztoła, D.; Niemczyk, M. P.; Wasielewski, M. R. *J. Am. Chem. Soc.* **1998**, *120*, 5118–5119. (e) Kelley, R. F.; Suk Shin, W.; Rybtchinski, B.; Sinks, L. E.; Wasielewski, M. R. *J. Am. Chem. Soc.* **2007**, *129*, 3173.
 (17) (a) Fukuzumi, S. In *Electron Transfer in Chemistry*; Balzani, V., Ed.; Wiley-VCH: Weinheim, 2001; Vol. 4, pp 3–67. (b) Fukuzumi, S.; Itoh, S. In *Advances in Photochemistry*; Neckers, D. C., Volman, D. H. von Büna, G., Eds.; Wiley: New York, 1998; Vol. 25, pp 107–172.
 (18) (a) Fukuzumi, S. *Bull. Chem. Soc. Jpn.* **1997**, *70*, 1. (b) Fukuzumi, S. *Org. Biomol. Chem.* **2003**, *1*, 609.
 (19) (a) Fukuzumi, S.; Koumitsu, S.; Hironaka, K.; Tanaka, T. *J. Am. Chem. Soc.* **1987**, *109*, 305. (b) Fukuzumi, S.; Nishizawa, N.; Tanaka, T. *J. Chem. Soc., Perkin Trans. 2* **1985**, 371–378.
 (20) (a) Fukuzumi, S.; Okamoto, T.; Otera, J. *J. Am. Chem. Soc.* **1994**, *116*, 5503. (b) Fukuzumi, S.; Satoh, N.; Okamoto, T.; Yasui, K.; Suenobu, T.; Seko, Y.; Fujitsuka, M.; Ito, O. *J. Am. Chem. Soc.* **2001**, *123*, 7756. (c) Fukuzumi, S.; Mori, H.; Imahori, H.; Suenobu, T.; Araki, Y.; Ito, O.; Kadish, K. M. *J. Am. Chem. Soc.* **2001**, *123*, 12458. (d) Fukuzumi, S.; Fujii, Y.; Suenobu, T. *J. Am. Chem. Soc.* **2001**, *123*, 10191.
 (21) (a) Fukuzumi, S.; Ohkubo, K.; Okamoto, T. *J. Am. Chem. Soc.* **2002**, *124*, 14147. (b) Fukuzumi, S.; Inada, O.; Satoh, N.; Suenobu, T.; Imahori, H. *J. Am. Chem. Soc.* **2002**, *124*, 9181. (c) Fukuzumi, S.; Yuasa, J.; Suenobu, T. *J. Am. Chem. Soc.* **2002**, *124*, 12566.
 (22) (a) Fukuzumi, S.; Okamoto, K.; Imahori, H. *Angew. Chem., Int. Ed.* **2002**, *41*, 620. (b) Fukuzumi, S.; Okamoto, K.; Yoshida, Y.; Imahori, H.; Araki, Y.; Ito, O. *J. Am. Chem. Soc.* **2003**, *125*, 1007.
 (23) (a) Fukuzumi, S.; Ohkubo, K. *Chem. Eur. J.* **2000**, *6*, 4532. (b) Fukuzumi, S.; Ohkubo, K. *J. Am. Chem. Soc.* **2002**, *124*, 10270.
 (24) Fukuzumi, S.; Ohkubo, K.; Ortiz, J.; Gutiérrez, A. M.; Fernández-Lázaro, F.; Sastre-Santos, A. *Chem. Commun.* **2005**, 3814.

- (25) Gaspard, S.; Maillard, P. *Tetrahedron* **1987**, *43*, 1083.
- (26) Demming, S.; Langhals, H. *Chem. Ber.* **1988**, *121*, 225.
- (27) Mann, C. K.; Barnes, K. K. *Electrochemical Reactions in Non-aqueous Systems*; Marcel Dekker: New York, 1990.
- (28) Becke, A. D. *J. Chem. Phys.* **1993**, *98*, 5648.
- (29) Lee, C.; Yang, W.; Parr, R. G. *Phys. Rev. B* **1988**, *37*, 785.
- (30) Hehre, W. J.; Radom, L.; Schleyer, P. v. R.; Pople, J. A. *Ab Initio Molecular Orbital Theory*; Wiley: New York, 1986.
- (31) Yilmaz, M. D.; Bozdemir, O. A.; Akkaya, E. U. *Org. Lett.* **2006**, *8*, 2871.
- (32) The triplet energy of zinc phthalocyanine has been reported:(a) Harriman, A.; Porter, G.; Richoux, M-C. *J. Chem. Soc., Faraday Trans.* **1971**, *55*, 4131. (b) Vincett, P. S.; Voight, E. M.; Rjeckhoff, K. E. *J. Chem. Phys.* **1971**, *55*, 4130. (c) Herkstroeter, W. G.; Merkel, P. B. *J. Photochem.* **1981**, *16*, 331.
- (33) The triplet energy of perylenediimide derivatives has been reported Ford, W. E.; Kamat, P. V. *J. Phys. Chem.* **1987**, *91*, 6373.
- (34) Gosztola, D.; Niemczyk, M. P.; Svec, W.; Lukas, A. S.; Wasielewski, M. R. *J. Phys. Chem. A* **2000**, *104*, 6545.
- (35) Dance, Z. E. X.; Mi, Q.; McCamant, D. W.; Ahrens, M. J.; Ratner, M. A.; Wasielewski, M. R. *J. Phys. Chem. B* **2006**, *110*, 25163.
- (36) van der Boom, T.; Hayes, R. T.; Zhao, Y.; Bushard, P. J.; Weiss, E. A.; Wasielewski, M. R. *J. Am. Chem. Soc.* **2002**, *124*, 9582.
- (37) Photoexcitation of zinc porphyrin–naphthalenediimide also affords the CS state, the lifetime of which can be altered by the coordination of metal ions to the naphthalenediimide moiety; see: Okamoto, K.; Mori, Y.; Yamada, H.; Imahori, H.; Fukuzumi, S. *Chem.-Eur. J.* **2004**, *10*, 474.
- (38) Fukuzumi, S.; Suenobu, T.; Patz, M.; Hirasaka, T.; Itoh, S.; Fujitsuka, M.; Ito, O. *J. Am. Chem. Soc.* **1998**, *120*, 8060.
- (39) No binding of Mg^{2+} to carbonyl oxygens of neutral quinones was observed, whereas the absorption bands of semiquinone radical anions were significantly shifted due to the complexation with Mg^{2+} ; see: Fukuzumi, S.; Ohkubo, K.; Okamoto, T. *J. Am. Chem. Soc.* **2002**, *124*, 14147.
- (40) The assignment of the *hfc* values of the $PDI^{\bullet-}-Mg^{2+}$ complex was made from the *hfc* ratio of the protonated $PDI^{\bullet-}$ [$(PDI-H)^{\bullet}$] calculated by DFT at the B3LYP/6-31G (d) basis set. The calculated *hfc* values of the $PDI^{\bullet-}-Mg^{2+}$ complex, which correspond to those in the gas phase, have failed to predict the observed *hfc* values in solution, because 99% of unpaired electron is calculated to be localized on Mg^{2+} nucleus.
- (41) (a) Fukuzumi, S.; Ohkubo, K.; Imahori, H.; Shao, J.; Ou, Z.; Zheng, G.; Chen, Y.; Pandey, R. K.; Fujitsuka, M.; Ito, O.; Kadish, K. M. *J. Am. Chem. Soc.* **2001**, *123*, 10676. (b) Kryatov, S. V.; Rybak-Akimova, E. V.; Schindler, S. *Chem. Rev.* **2005**, *105*, 2175.

JP805464E